Passive Radar Imaging of Moving Targets in Multiple-Scattering Environments Using Sparse Distributed Apertures

Ling Wang
College of Electronic and Information Engineering
Nanjing University of Aeronautics and Astronautics
Nanjing 210016, China
Email: wanglrpi@gmail.com

Birsen Yazıcı**
Department of Electrical, Computer and Systems Engineering,
Rensselaer Polytechnic Institute,
110 8th Street, Troy, NY 12180 USA
Email: yazici@ecse.rpi.edu

***Abstract*—We present a novel passive image formation method for moving targets using sparse distributed apertures in multiple-scattering environments and non-cooperative sources of opportunity. This method is capable of exploiting information about multiple-scattering in the environment. We develop a passive measurement model that relates measurements at a given receiver to measurements at other receivers. We address the passive imaging problem as a generalized likelihood ratio test for a hypothetical target located at an unknown position, moving with an unknown velocity. We design a linear discriminant functional by maximizing the signal-to-noise ratio of the test-statistic and use the resulting position- and velocity-resolved test-statistic to form the image. We perform numerical simulations to demonstrate the performance of our passive imaging method operating in multiple-scattering environments.**

***Index Terms*—Passive Radar, Imaging, Moving target, Distributed apertures, Multiple-Scattering, Generalized likelihood ratio test**

I. Introduction

Passive radar imaging of moving targets is concerned with determining the position and velocity of objects using the scattered wave field measurements due to illumination sources of opportunity. In recent years, the growing availability of radio frequency illumination sources of opportunity, such as broadcasting and television stations, cell phone stations, has motivated interest in passive radar imaging.

A number of passive detection and imaging approaches have been proposed in the literature [1]–[10]. Most of these techniques implicitly assume a single-scattering environment. However, urban areas are typically multiple-scattering environments.

In [11] we presented a novel passive imaging method using sparse distributed apertures. This method assumes that the targets are at rest during the transmission and the corresponding reception and focuses on the reconstruction of the distribution of targets in the *position space only*. In this paper, we use the framework introduced in [11] and present a passive imaging method for moving targets using sparse distributed apertures to reconstruct the distribution of targets in *both position and velocity spaces*. To the best of our knowledge, our method is the first in the literature that exploits information about multiple-scattering for imaging of moving targets.

We derive a passive measurement model which relates the Doppler as well as delay information measured at a receiver location to the delay and Doppler information measured at other receiver locations due to a hypothetical moving target in position and velocity spaces. We formulate the imaging problem as a Generalized Likelihood Ratio Test (GLRT) with unknown target location and unknown velocity. The GLRT is a particularly suitable framework for the sparse arrays due to limited aperture available. Our method determines the two- or three-dimensional velocity information as well as two- or three-dimensional position of the moving target and requires no information on the location of transmitters or the transmitted waveforms.

While we focus specially on passive radar imaging, our method is also applicable to passive microwave, seismic or acoustic imaging.

This work was supported by the Air Force Office of Scientific Research (AFOSR) under the agreements FA9550-07-1-0363 and FA9550-09-1-0013 and National Science Foundation (NSF) under Grant No. CCF-08030672.

** Corresponding author

II. Passive Measurement Model

We reserve $\mathbf{x}$ to denote location in 3D Euclidean space and $\boldsymbol{x}$ to denote location in 2D space. We denote operators $(\mathcal{G}, \mathcal{R}, \text{etc.})$ with calligraphic letters. For a function f, $\hat{f}$ denotes its Fourier transform and f^* denotes its complex conjugate. Bold font denotes vector quantities. Non-bold italic font denotes scalar quantities.

A. Model for the scattered field

The propagation of electromagnetic waves due to an arbitrary source distribution $s(\mathbf{x}, t)$ in a medium can be described using the scalar wave equation [12]–[14]:

$$[\nabla^2 - c^{-2}(\mathbf{x}, t)\partial_t^2]E(\mathbf{x}, t) = s(\mathbf{x}, t) \tag{1}$$

where c is the wave speed in the medium and E is the electric field. The propagation medium is characterized by the *Green's*

function satisfying

$$[\nabla^2 - c_0^{-2}\partial_t^2]g(\mathbf{x},\mathbf{z},t) = \delta(\mathbf{x}-\mathbf{z})\delta(t)\,. \tag{2}$$

The wave speed c can be expressed in terms of the background propagation speed and the perturbation due to deviation from the background reflectivity. Let $q_{\mathbf{v}}$ denote the *phase-space* distribution, at time $t = 0$, of scatterers moving with velocity $\mathbf{v}$. The moving scatterers in the spatial volume d^3x (at $\mathbf{x}$) give rise to $c^{-2}(t,\mathbf{x}) = c_0^{-2} + \int q_{\mathbf{v}}(\mathbf{x}-\mathbf{v}t)d\mathbf{v}$ [15].

We assume that the electromagnetic waves decay rapidly as they penetrate the ground [16]. We then write $q_{\mathbf{v}}(\mathbf{x}-\mathbf{v}t)$ in terms of the two-dimensional location and two-dimensional velocity as follows:

$$q_{\mathbf{v}}(\mathbf{x}-\mathbf{v}t) = q_{\boldsymbol{v}}(\boldsymbol{x}-\boldsymbol{v}t)\delta(x_3 - h(\boldsymbol{x}))\delta(v_3 - Dh(\boldsymbol{x})\cdot\boldsymbol{v}) \tag{3}$$

where $\mathbf{x} = (\boldsymbol{x}, x_3), \boldsymbol{x} \in \mathbb{R}^2$ and $\mathbf{v} = (\boldsymbol{v}, v_3), \boldsymbol{v} \in \mathbb{R}^2$, $h : \mathbb{R}^2 \to \mathbb{R}$ represents the ground topography and $Dh(\boldsymbol{x}) = [\frac{\partial h}{\partial x_1} \quad \frac{\partial h}{\partial x_2}]$.

Let E^{sc} denote the scattered field due to the moving perturbation $q_{\boldsymbol{v}}$. Then, under the Born approximation [17], the scattered field is modeled as

$$E^{\mathrm{sc}}(\mathbf{x},t) = \int g(\mathbf{x},\boldsymbol{y},t-\tau)q_{\boldsymbol{v}}(\boldsymbol{y}-\boldsymbol{v}\tau)\partial_\tau^2 E^{\mathrm{in}}(\boldsymbol{y},\tau)d\tau d\boldsymbol{y}d\boldsymbol{v} \tag{4}$$

where we define $g(\mathbf{x},\boldsymbol{y},t)$ as the 3D Green's function of the background environment that is equal to $g(\mathbf{x},(\boldsymbol{y},h(\boldsymbol{y})),t)$. E^{in} denotes the incident field due to the source distribution $s(\mathbf{x},t)$ modeled as

$$E^{\mathrm{in}}(\boldsymbol{y},t) = \int g(\boldsymbol{y},\mathbf{z},t-\tau)s(\mathbf{z},\tau)d\tau d\mathbf{z} \tag{5}$$

where $g(\boldsymbol{y},\mathbf{z},t)$ is the 3D Green's function defined as $g((\boldsymbol{y},h(\boldsymbol{y})),\mathbf{z},t)$.

For multiple transmitters with isotropic antennas, say M, the source distribution can be expressed as $s(\mathbf{x},t) = \sum_{q=1}^{M}\delta(\mathbf{x}-\mathbf{z}_q)p_q(t+T_{\mathbf{z}_q})$ where $\mathbf{z}_q, q = 1,\cdots,M$ denotes the location of the q^{th} transmitter transmitting the waveform $\hat{p}_q$ starting at time $t = -T_{\mathbf{z}_q}$. Thus, (5) can be expressed as

$$E^{\mathrm{in}}(\boldsymbol{y},t) = \sum_{q=1}^{M}\int \underbrace{g(\boldsymbol{y},\mathbf{z}_q,t-\tau)p_q(\tau+T_{\mathbf{z}_q})}_{E_q^{\mathrm{in}}(\boldsymbol{y},\mathbf{z}_q,t)}d\tau \tag{6}$$

where E_q^{in} represents the incident field on the target due to the q^{th} transmitter. Note that the isotropic antenna assumption is not necessary for the rest of our development. The results in the following sections can be extended to incorporate realistic antenna models in a straightforward manner.

B. Measurement Model

For multiple-scattering environments, we consider a multi-bounce, multiple-scattering environment model [11], [18], [19]. We assume that there are L point scatterers in the background medium and consider only the propagation paths originating from the target to a background scatterer or from the background scatterer to the receiver. This results in L multipath bounces between the target and background

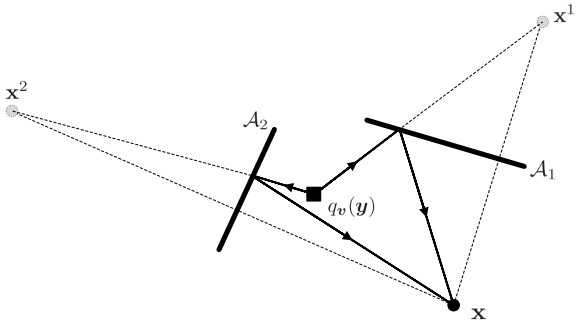

Fig. 1. An illustration of the mirror receivers in 2D space. $\mathbf{x}$ denotes the receiver location. $\mathbf{x}^l$ $(l = 1, 2)$ denote mirror receivers with respect to the the mirror planes $\mathcal{A}_l, (l = 1, 2)$, respectively. $q_{\boldsymbol{v}}(\boldsymbol{y})$ denotes the target.

medium. We further assume that all multipath bounces are specular reflections and therefore model the environment as a collection of mirror planes. In this case, the Green's function of the background can be approximated by a shoot-and-bounce model [20]:

$$\hat{g}(\mathbf{x},\mathbf{y},\omega) = \frac{\mathrm{e}^{-\mathrm{i}k|\mathbf{x}-\mathbf{y}|}}{4\pi|\mathbf{x}-\mathbf{y}|} + \sum_{l=1}^{L} a_l \frac{\mathrm{e}^{-\mathrm{i}k|\mathbf{x}^l-\mathbf{y}|}}{4\pi|\mathbf{x}^l-\mathbf{y}|} \tag{7}$$

$$= \sum_{l=0}^{L} a_l \frac{\mathrm{e}^{-\mathrm{i}k|\mathbf{x}^l-\mathbf{y}|}}{4\pi|\mathbf{x}^l-\mathbf{y}|}, \quad a_0 = 1,\ \mathbf{x}^0 = \mathbf{x} \tag{8}$$

where $k = \omega/c_0$, $\mathbf{x}^l$ is reflection of $\mathbf{x}$ about the mirror plane, $\mathcal{A}_l$ with respect to the $l\mathrm{th}, (l = 1,\cdots,L)$ multipath bounce and a_l are the corresponding attenuation coefficients. We define the receivers located at $\mathbf{x}^l, (l = 1,\cdots,L)$ as *mirror receivers*. Fig. 1 illustrates the concept of mirror receivers in two-dimensional space.

(8) allows us to readily compare the Point Spread Function (PSF) of the imaging operator obtained for free-space to those for the multiple-scattering environment. (8) can be expressed as

$$\hat{g}(\mathbf{x},\mathbf{y},\omega) = \sum_{l=0}^{L} a_l \hat{g}_0(\mathbf{x}^l,\mathbf{y},\omega) \tag{9}$$

where $\hat{g}_0$ denotes the Fourier transform of the free-space Green's function given by

$$\hat{g}_0(\mathbf{x}^l,\mathbf{y},\omega) = \frac{\mathrm{e}^{-\mathrm{i}k|\mathbf{x}^l-\mathbf{y}|}}{4\pi|\mathbf{x}^l-\mathbf{y}|}. \tag{10}$$

Since in free-space, the measurement model in Fourier domain is given as follows [21]:

$$\hat{m}(\omega) = \int \hat{g}_0(\mathbf{x}_0,\boldsymbol{y},\omega)q_{\boldsymbol{v}}(\boldsymbol{y})\mu^2_{\boldsymbol{y},\boldsymbol{v},\mathbf{x}_0}\omega^2 \times \hat{\tilde{E}}^{\mathrm{in}}(\boldsymbol{y},\mu_{\boldsymbol{y},\boldsymbol{v},\mathbf{x}_0}\omega)d\boldsymbol{y}d\boldsymbol{v} + \hat{n}(\omega) \tag{11}$$

where n is zero-mean with finite second-order statistics and

$$\hat{\tilde{E}}^{\mathrm{in}}(\boldsymbol{y},\omega) = -\sum_{q=1}^{M}\frac{1}{\tilde{\mu}^2_{\boldsymbol{y},\boldsymbol{v},\mathbf{z}_q}}\hat{E}_q^{\mathrm{in}}(\boldsymbol{y},\mathbf{z}_q,\frac{\omega}{\tilde{\mu}_{\boldsymbol{y},\boldsymbol{v},\mathbf{z}_q}}) \tag{12}$$

with

$$\hat{E}_q^{\text{in}}(\boldsymbol{y}, \mathbf{z}_q, \frac{\omega}{\tilde{\mu}_{\boldsymbol{y},\boldsymbol{v},\mathbf{z}_q}}) = \frac{1}{\tilde{\mu}_{\boldsymbol{y},\boldsymbol{v},\mathbf{z}_q}} \hat{g}_0(\mathbf{y}, \mathbf{z}, \frac{\omega}{\tilde{\mu}_{\boldsymbol{y},\boldsymbol{v},\mathbf{z}_q}}) \times \hat{p}_q(\frac{\omega}{\tilde{\mu}_{\boldsymbol{y},\boldsymbol{v},\mathbf{z}_q}}) \mathrm{e}^{\mathrm{i}\frac{\omega}{\tilde{\mu}_{\boldsymbol{y},\boldsymbol{v},\mathbf{z}_q}} T_{\mathbf{z}_q}}, \quad (13)$$

the measurement model in multiple-scattering environment can be expressed as

$$\hat{m}(\omega) = \sum_{l=0}^{L} a_l \int \hat{g}_0(\mathbf{x}^l, \boldsymbol{y}, \omega) q_{\boldsymbol{v}}(\boldsymbol{y}) \mu^2_{\boldsymbol{y},\boldsymbol{v},\mathbf{x}^l} \omega^2 \times \hat{\tilde{E}}^{\text{in}}(\boldsymbol{y}, \mu_{\boldsymbol{y},\boldsymbol{v},\mathbf{x}^l}\omega) d\boldsymbol{y} d\boldsymbol{v} + \hat{n}(\omega) \quad (14)$$

where

$$\hat{\tilde{E}}^{\text{in}}(\boldsymbol{y}, \omega) = -\sum_{q=1}^{M}\sum_{\nu=1}^{L} \frac{1}{\tilde{\mu}^2_{\boldsymbol{y},\boldsymbol{v},\mathbf{z}_q^\nu}} \hat{E}_q^{\text{in}}(\boldsymbol{y}, \mathbf{z}_q^\nu, \frac{\omega}{\tilde{\mu}_{\boldsymbol{y},\boldsymbol{v},\mathbf{z}_q^\nu}}). \quad (15)$$

In (15), $\mathbf{z}_q^0 = \mathbf{z}_q$ and $\mathbf{z}_q^\nu, \nu = 1, \cdots, L$ are the reflections of the transmitters located at $\mathbf{z}_q$ about the plane $\mathcal{A}_\nu$. We refer to these transmitters as *mirror transmitters*. $\hat{E}_q^{\text{in}}(\boldsymbol{y}, \mathbf{z}_q^\nu, \omega/\tilde{\mu}_{\boldsymbol{y},\boldsymbol{v},\mathbf{z}_q^\nu})$ is given in (13) with $\mathbf{z}_q$ replaced with $\mathbf{z}_q^\nu$.

In (14) and (15), $\mu_{\boldsymbol{y},\boldsymbol{v},\mathbf{x}^l}$ is given by

$$\mu_{\boldsymbol{y},\boldsymbol{v},\mathbf{x}^l} = 1 + \widehat{\mathbf{y} - \mathbf{x}^l} \cdot \mathbf{v}/c_0\,, \quad (16)$$

which denotes the *Doppler-scale-factor observed at location* $\mathbf{x}$ *due to a moving target* [11] with velocity $\boldsymbol{v}$ at location $\boldsymbol{y}$ associated with the l^{th} multipath propagation. $\tilde{\mu}_{\boldsymbol{y},\boldsymbol{v},\mathbf{z}_q^\nu}$ is given by

$$\tilde{\mu}_{\boldsymbol{y},\boldsymbol{v},\mathbf{z}_q^\nu} = 1 - \widehat{\mathbf{y} - \mathbf{z}_q^\nu} \cdot \mathbf{v}/c_0\,, \quad (17)$$

which denotes the *Doppler-scale-factor observed by the moving target* [11] located at $\boldsymbol{y}$ moving with velocity $\boldsymbol{v}$ due to a waveform transmitted from $\mathbf{z}_q$ along the ν^{th} multipath bounce.

C. Passive measurement model

In the analysis that follows, we consider a sparse distribution of N receivers located at $\mathbf{x}_i\,, i = 1, \cdots, N$ and M transmitters located at $\mathbf{z}_q\, i = 1, \cdots, M$. The receivers and transmitters may be arbitrarily located with several hundred wavelengths apart with no assumption that transmitters and receivers are colocated. Fig. 2 illustrates the imaging scenario that is considered. Non-identical waveforms may be transmitted from different transmitters.

For passive detection and imaging applications, the information of the transmitted waveforms and the location of the transmitters may not be available. We develop an alternative passive measurement model that expresses measurements at each receiver in terms of the measurements at a different receiver. This model is based on the fact that the measurements at all receiver are due to the same incident field $\tilde{E}^{\text{in}}$, target velocity and phase space distribution. The model involves back propagating the measurement at a receiver location to a hypothetical target location moving at a hypothetical velocity and then forward propagating the resulting field to another receiver location.

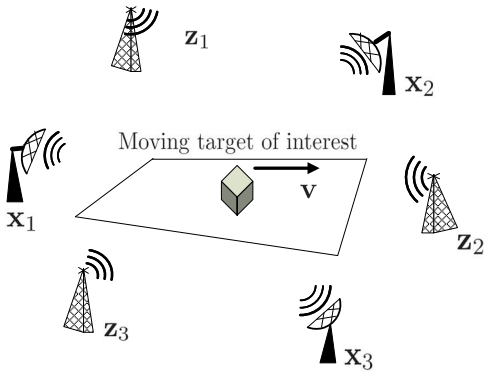

Fig. 2. The figure illustrates a typical distributed aperture setup with receive and transmit antenna elements that are several hundred wavelengths apart. $\mathbf{x}_i\ (i = 1, \cdots, 3)$ denote receivers and $\mathbf{z}_i\ (i = 1, \cdots, 3)$ denote transmitters.

We use (14) to define the forward-propagation operator, $\mathcal{P}_{\boldsymbol{y},\boldsymbol{v},i}$, with respect to the i^{th} receiver as follows:

$$\mathcal{P}_{\boldsymbol{y},\boldsymbol{v},i}[u](\omega) = \sum_{l=0}^{L} a_l \mathcal{G}^l_{\boldsymbol{y},i} \mathcal{S}^l_{\boldsymbol{v},i}[u](\omega) \quad (18)$$

where

$$u(\boldsymbol{y}, \boldsymbol{v}, \omega) = q_{\boldsymbol{v}}(\boldsymbol{y}) \omega^2 \hat{\tilde{E}}^{\text{in}}(\boldsymbol{y}, \omega), \quad (19)$$

$\mathcal{S}^l_{\boldsymbol{v},i}$ is the scaling operator that accounts for the Doppler effect observed by the i^{in} receiver due to a moving target with velocity $\boldsymbol{v}$ at location $\boldsymbol{y}$ associated with the l^{th}, $l = 1, \cdots, L$ multipath bounce; $\mathcal{G}^l_{\boldsymbol{y},i}$ is the operator that accounts for the wave propagation in the stationary background from the target to the i^{th} receiver via the l^{th}, $l = 1, \cdots, L$ multipath bounce; and a_l is the corresponding attenuation coefficient defined as above. Note that in (19), u is viewed as a function of ω only, and $\boldsymbol{y}$ and $\boldsymbol{v}$ are fixed parameters.

We assume that the moving target is composed of a collection of point targets in position and velocity spaces. Then, we define $\mathcal{S}^l_{\boldsymbol{v},i}$, $l = 0, \cdots, L$ as

$$\mathcal{S}^l_{\boldsymbol{v},i}[u](\omega) = \mu_{\boldsymbol{y},\boldsymbol{v},\mathbf{x}_i^l}\, u(\boldsymbol{y}, \boldsymbol{v}, \mu_{\boldsymbol{y},\boldsymbol{v},\mathbf{x}_i^l}\, \omega) \quad (20)$$

and define $\mathcal{G}^l_{\boldsymbol{y},i}$, $l = 0, \cdots, L$ as

$$\mathcal{G}^l_{\boldsymbol{y},i}[u](\omega) = \hat{g}_0(\mathbf{x}_i^l, \boldsymbol{y}, \omega) u(\boldsymbol{y}, \boldsymbol{v}, \omega) \quad (21)$$

where $\hat{g}_0(\mathbf{x}_i^l, \boldsymbol{y}, \omega)$ is the Fourier transform of the 3D free-space Green's function $g_0(\mathbf{x}_i^l, (\boldsymbol{y}, h(\boldsymbol{y})), t)$ given in (10).

We define the back-propagation operator as the adjoint of $\mathcal{P}_{\boldsymbol{y},\boldsymbol{v},i}$ and denote it with $\mathcal{P}^\dagger_{\boldsymbol{y},\boldsymbol{v},i}$. Using (18), we express $\mathcal{P}^\dagger_{\boldsymbol{y},\boldsymbol{v},i}$ as

$$\mathcal{P}^\dagger_{\boldsymbol{y},\boldsymbol{v},i} = \sum_{l=0}^{L} a_l^* \mathcal{S}^{l,\dagger}_{\boldsymbol{v},i} \mathcal{G}^{l,\dagger}_{\boldsymbol{y},i} \quad (22)$$

where $\mathcal{S}^{l,\dagger}_{\boldsymbol{v},i}$ and $\mathcal{G}^{l,\dagger}_{\boldsymbol{y},i}$ are the adjoint of $\mathcal{S}^l_{\boldsymbol{v},i}$ and $\mathcal{G}^l_{\boldsymbol{y},i}$, respectively.

Let $\hat{m}_i$ denote the measurement at the i^{th} receiver. We can now express the measurement, $\hat{m}_i$, at the i^{th} receiver in terms of the measurement, $\hat{m}_j$, at the j^{th} receiver by back-propagating $\hat{m}_j$ measured at $\mathbf{x}_j$ to a hypothetical target

location with a hypothetical velocity via the back-propagation operator; and then forward propagating the resulting field to $\mathbf{x}_i$ via the forward-propagation operator. Note that in the back-propagation operation, not only the noise-free measurement but also the noise at the j^{th} receiver are back-propagated. Thus, we have

$$\hat{m}_i(\omega) = \mathcal{P}_{\boldsymbol{y},\boldsymbol{v},i}\mathcal{P}^{\dagger}_{\boldsymbol{y},\boldsymbol{v},j}\hat{m}_j(\omega) + \hat{n}_i(\omega). \tag{23}$$

For a moving point target model given by

$$q_{\boldsymbol{v}}(\boldsymbol{y}) = \rho\,\delta(\boldsymbol{y}-\boldsymbol{y}_0)\delta(\boldsymbol{v}-\boldsymbol{v}_0) \tag{24}$$

where ρ is the reflectivity of the point target located at $\boldsymbol{y}_0$, at time $t=0$, moving with velocity $\boldsymbol{v}_0$, the forward-propagating operator in (18) reduces to

$$\begin{aligned}\mathcal{P}_{\boldsymbol{y}_0,\boldsymbol{v}_0,i}[u](\omega) = \sum_{l=0}^{L} a_l \hat{g}_0(\mathbf{x}_i^l, \boldsymbol{y}_0, \omega) \\ \times \mu_{\boldsymbol{y}_0,\boldsymbol{v}_0,\mathbf{x}_i^l}\hat{u}(\mu_{\boldsymbol{y}_0,\boldsymbol{v}_0,\mathbf{x}_i^l},\omega)\,.\end{aligned} \tag{25}$$

The back-propagation operator in (22) becomes

$$\begin{aligned}\mathcal{P}^{\dagger}_{\boldsymbol{y}_0,\boldsymbol{v}_0,i}[\hat{m}_i](\omega) = \sum_{l=0}^{L} a_l^* \hat{m}_i\left(\frac{\omega}{\mu_{\boldsymbol{y}_0,\boldsymbol{v}_0,\mathbf{x}_i^l}}\right) \\ \times \hat{g}_0^*\left(\mathbf{x}_i^l, \boldsymbol{y}_0, \frac{\omega}{\mu_{\boldsymbol{y}_0,\boldsymbol{v}_0,\mathbf{x}_i^l}}\right).\end{aligned} \tag{26}$$

Using (25) and (26), for a moving point target, (23) becomes

$$\begin{aligned}\hat{m}_i(\omega) = \sum_{l,l'=0}^{L} a_l a_{l'}^* \hat{g}_0(\mathbf{x}_i^l, \boldsymbol{y}_0, \omega)\hat{g}_0^*(\mathbf{x}_j^{l'}, \boldsymbol{y}_0, \gamma^{ij,\beta}_{\boldsymbol{y}_0,\boldsymbol{v}_0}\,\omega) \\ \times \mu_{\boldsymbol{y}_0,\boldsymbol{v}_0,\mathbf{x}_i^l}\hat{m}_j(\gamma^{ij,\beta}_{\boldsymbol{y}_0,\boldsymbol{v}_0}\,\omega) + \hat{n}_i(\omega)\end{aligned} \tag{27}$$

where $\gamma^{ij,\beta}_{\boldsymbol{y}_0,\boldsymbol{v}_0}, \beta = (l,l')$ is the ratio of the Doppler-scale-factors associated with the multipath propagation between the target and the i^{th} and j^{th} receivers. It has the form

$$\gamma^{ij,\beta}_{\boldsymbol{y}_0,\boldsymbol{v}_0} := \frac{\mu_{\boldsymbol{y}_0,\boldsymbol{v}_0,\mathbf{x}_i^l}}{\mu_{\boldsymbol{y}_0,\boldsymbol{v}_0,\mathbf{x}_j^{l'}}} = \frac{1+\widehat{\mathbf{y}_0-\mathbf{x}_i^l}\cdot\mathbf{v}_0/c_0}{1+\widehat{\mathbf{y}_0-\mathbf{x}_j^{l'}}\cdot\mathbf{v}_0/c_0}\,, \quad \beta=(l,l') \tag{28}$$

Note that $\mathbf{y}_0 = (\boldsymbol{y}_0, h(\boldsymbol{y}_0))$ and $\mathbf{v}_0 = (\boldsymbol{v}_0, Dh(\boldsymbol{y}_0)\cdot\boldsymbol{v}_0)$. We refer to $\gamma^{ij,\beta}_{\boldsymbol{y}_0,\boldsymbol{v}_0}, \beta=(l,l')$ as the *passive-Doppler-scale-factor* for the i^{th} and j^{th} receivers due to $l^{\text{th}}, l'^{\text{th}}$ multipath bounces.

Substituting the Fourier transform of the free-space Green's function into (27), we obtain

$$\begin{aligned}\hat{m}_i(\omega) = \sum_{l,l'=0}^{L} \frac{a_l a_{l'}^* \mu_{\boldsymbol{y}_0,\boldsymbol{v}_0,\mathbf{x}_i^l}}{(4\pi)^2|\mathbf{x}_j^{l'}-\mathbf{y}_0||\mathbf{x}_i^l-\mathbf{y}_0|} \\ \times \mathrm{e}^{-\mathrm{i}k(|\mathbf{x}_i^l-\mathbf{y}_0|-\gamma^{ij,\beta}_{\boldsymbol{y}_0,\boldsymbol{v}_0}|\mathbf{x}_j^{l'}-\mathbf{y}_0|)} \\ \times \hat{m}_j(\gamma^{ij,\beta}_{\boldsymbol{y}_0,\boldsymbol{v}_0}\,\omega) + \hat{n}_i(\omega)\,.\end{aligned} \tag{29}$$

We next form a vector measurement model by taking one of the receivers as a reference. Without loss of generality, we take the j^{th} receiver as a reference and form the following measurement vector:

$$\mathbf{m} = \begin{bmatrix} \hat{m}_1 & \hat{m}_2 & \cdots & \hat{m}_N \end{bmatrix}^T. \tag{30}$$

Similarly, we can vectorize the "reference measurements" and the noise as follows:

$$\mathbf{m_r} = \begin{bmatrix} \hat{m}_j & \hat{m}_j & \cdots & \hat{m}_j \end{bmatrix}^T \tag{31}$$

$$\mathbf{n} = \begin{bmatrix} \hat{n}_1 & \hat{n}_2 & \cdots & \hat{n}_N \end{bmatrix}^T \tag{32}$$

where $\hat{n}_i, i\neq j$ is the additive thermal noise at the i^{th} receiver. Note that $\mathbf{m}, \mathbf{m_r}$ and $\mathbf{n}$ are all $(N-1)$ dimensional vectors.

The composition of the back-propagation and forward-propagation operators can be represented as a diagonal matrix given by

$$\mathbf{P}_{\boldsymbol{y},\boldsymbol{v}} = \mathrm{diag}\begin{bmatrix} \mathcal{P}_{\boldsymbol{y},\boldsymbol{v},1}\mathcal{P}^{\dagger}_{\boldsymbol{y},\boldsymbol{v},j} & \cdots & \mathcal{P}_{\boldsymbol{y},\boldsymbol{v},N}\mathcal{P}^{\dagger}_{\boldsymbol{y},\boldsymbol{v},j} \end{bmatrix} \tag{33}$$

where $i\neq j$ and $\mathbf{P}_{\boldsymbol{y},\boldsymbol{v}}$ is $(N-1)\times(N-1)$.

Using (23), (30)-(33), we form a vectorized passive measurement model as follows:

$$\mathbf{m}(\omega) = \mathbf{P}_{\boldsymbol{y},\boldsymbol{v}}\mathbf{m_r}(\omega) + \mathbf{n}(\omega) \tag{34}$$

for some range of ω. Note that in (34), all operations are understood to be elementwise.

III. Image Formation

We use a hypothesis testing based approach to address the passive imaging problem, which has its root in the Generalized Likelihood Ratio Test (GLRT) [22], [23]. We set up a position- and velocity-resolved binary hypothesis testing and next determine a test-statistic for each location $(\boldsymbol{y}, h(\boldsymbol{y})) \in \mathbb{R}^3$ and each velocity $(\boldsymbol{v}, Dh(\boldsymbol{y})\cdot\boldsymbol{v}) \in \mathbb{R}^3$ in the position and velocity spaces using the passive measurement model for moving targets developed in subsection II-C. The image is then formed in the $(\boldsymbol{y},\boldsymbol{v})$ domain with the position- and velocity-resolved test-statistic.

We consider the following test of binary hypothesis for each location and velocity in $(\boldsymbol{y},\boldsymbol{v})$ space:

$$\begin{aligned}\mathcal{H}_0 :&\quad \mathbf{m} = \mathbf{n} \\ \mathcal{H}_1 :&\quad \mathbf{m} = \mathbf{P}_{\boldsymbol{y},\boldsymbol{v}}\mathbf{m_r} + \mathbf{n}\end{aligned} \tag{35}$$

where $\mathbf{P}_{\boldsymbol{y},\boldsymbol{v}}, \mathbf{m_r}, \mathbf{m}$ and $\mathbf{n}$ are as defined in (30)-(34).

The null hypothesis states that the measurement is due to noise whereas the alternative hypothesis states that the measurement is due to a target located at $\boldsymbol{y}$ moving with velocity $\boldsymbol{v}$.

We design a linear discriminant functional to address the binary hypothesis testing problem,

$$\lambda = \langle \mathbf{m}, \mathbf{w}\rangle := \int \mathbf{w}^H \mathbf{m} d\omega = \sum_{i,i\neq j}\int w_i^*(\omega)\hat{m}_i(\omega)d\omega \tag{36}$$

where λ denote the the output of the discriminant functional, which we call the *test-statistic*, and $\mathbf{w}$ is a template given by

$$\mathbf{w} = \begin{bmatrix} w_1 & w_2 & \cdots & w_N \end{bmatrix}^T. \tag{37}$$

We determine the test-statistic by maximizing the Signal-to-Noise Ratio (SNR) of λ. Under the assumption that the noise at different receivers are wide sense stationary and mutually uncorrelated, the resulting optimal linear template is given by

$$\mathbf{w}_{\text{opt}} = \overline{\mathbf{S}}^{-1}\mathbf{P}_{\boldsymbol{y},\boldsymbol{v}}\overline{\mathbf{m}}_{\mathbf{r}} \tag{38}$$

where $\overline{\mathbf{S}}^{-1}$ is the inverse of $\overline{\mathbf{S}}$ defined by

$$\overline{\mathbf{S}}(\omega) = \int 1/2(\mathbf{R}_1(\omega,\omega') + \mathbf{R}_0(\omega,\omega'))d\omega' \qquad (39)$$

with $\mathbf{R}_0 = \mathrm{Cov}\,[\mathbf{m}|\mathcal{H}_0]$ and $\mathbf{R}_1 = \mathrm{Cov}\,[\mathbf{m}|\mathcal{H}_1]$ where Cov denotes the covariance operator. One can show that $\overline{\mathbf{S}}^{-1}$ can be approximated by a diagonal matrix. We denote diagonal elements of $\overline{\mathbf{S}}^{-1}$ by $\overline{S}_i^{-1}(\omega), i = 1, \cdots, N$ and $i \neq j$, which is a function of the power spectral density function of noise at the i^{th} receiver and the kernel of $\mathbf{P}_{\boldsymbol{y},\boldsymbol{v}}$. (38) shows that the optimal template is position and velocity dependent.

IV. Numerical Simulations

A. Settings

We conducted numerical simulations to verify the theory and demonstrate the performance of our passive imaging method using a moving point target model.

We considered a scene of size $[0, 3\text{e}3] \times [0, 3\text{e}3]\,\text{m}^2$ with flat topography. We discretized the scene into 201×201 pixels where $[0, 0, 0]\,\text{m}$ and $[3\text{e}3, 3\text{e}3, 0]\,\text{m}$ correspond to the pixels $(1, 1)$ and $(201, 201)$, respectively. We assumed that the target velocity was in the range of $[-20, 20] \times [-20, 20]\,\text{m/s}$. We discretized the velocity plane into 401×401 pixels where $[-20, -20, 0]\,\text{m}$ and $[20, 20, 0]\,\text{m}$ correspond to the pixels $(1, 1)$ and $(401, 401)$, respectively.

The point target with unit reflectivity was assumed to be located at $[2.5\text{e}3 \quad 2\text{e}3 \quad 0]^T\,\text{m}$ moving with velocity $[-10, 15]\,\text{m/s}$.

We assumed that there were five receivers and a single transmitter present in the scene. The single transmitter was assumed to be located at $[1.5\text{e}3, 0, 6]^T\,\text{m}$. The receivers were assumed to lie on the x-axis, equidistant form each other in the range of $[0, 3\text{e}3]^T\,\text{m}$. Both the transmitter and receivers were assumed to be on the same plane, $y_3 = 6\text{m}$.

We considered a specular reflecting wall located at $y_1 = 0$. Thus, the multiple-scattering environment was modeled with the shoot-and-bounce model with one extra path.

In all the experiments, the noise was simulated as the additive white Gaussian process.

We perform the image reconstruction using a waveform that has high Doppler resolution and good range resolution. Examples for such waveforms include wireless network (or WiFi) signals, Digital Video Broadcasting Terrestrial (DVB-T) signals and WiMAX [24] waveforms which have relatively large bandwidth that can offer reasonable range resolution. We refer to such waveforms as the high-Doppler and good-range resolution waveforms. We simulated a high-Doppler and good-range resolution waveform as a continuous-wave (CW) with 4GHz carrier frequency, 0.1s duration and an additional frequency modulation, which results in a bandwidth of 7.5MHz. Such a waveform provides about $19.5\,\text{m}$ range resolution, and $0.375\,\text{m/s}$ radial velocity resolution in monostatic operations.

We reconstructed the four-dimensional test-statistic image in $(\boldsymbol{y}, \boldsymbol{v})$ (or (y_1, y_2, v_1, v_2)) coordinates. However, in order to facilitate visualization and performance evaluation, we generated three two-dimensional images from the original four dimensional image: The fist image, which we refer to as the peak-value image, was generated by choosing the maximum value of the four-dimensional image for each velocity (v_1, v_2). We then, choose the maximum value, $\tilde{\boldsymbol{v}}$, of the peak-value image as the estimate of the velocity. The second image, which we refer to as the position-image, is the cross-section of the four-dimensional image, for $\boldsymbol{v} = \tilde{\boldsymbol{v}}$. We take the maximum value, $\tilde{\boldsymbol{y}}$, of the position-image as the estimate of the target's position. The third image, which we refer to as the velocity-image, is the cross-section of the four-dimensional image, for $\boldsymbol{y} = \tilde{\boldsymbol{y}}$.

B. Results

The reconstructed images in multiple-scattering environments using a high-Doppler and good-range resolution waveform are shown in Fig. 3. We see that in multiple-scattering environments, the target is reconstructed at the correct location with correct velocity. As compared to the image reconstructed in free-space [21], the strength of the reconstructed target increases when we exploited the multipath effect. However, there are also additional artifacts present in the background of the reconstructed images, which degrades the contrast of the images.

V. Conclusion

In this work, we developed a new passive radar imaging method for moving targets using sparsely distributed receivers. This method is capable of exploiting the multiple-scattering. The numerical simulations conducted in multiple-scattering environments using the waveforms available in practice demonstrate the performance of our imaging method.

A detailed resolution analysis of the proposed method will be presented in the future.

While we mainly focused on passive radar application, the results presented in our paper are also applicable to other wave-based passive imaging applications, such as those in passive acoustic or seismic imaging.

References

[1] H. D. Griffiths and C. J. Baker, "Passive coherent location radar systems. part 1: Performance prediction," *IEE Proceedings of Radar, Sonar and Navigation*, vol. 152, no. 3, pp. 153–159, June 2005.

[2] D. W. O'Hagan and C. J. Baker, "Passive bistatic radar (PBR) using FM radio illuminators of opportunity," in *Proc. of 2008 IEEE Radar Conference, Roma, Italy*, May 2008.

[3] D. Poullin, "Passive detection using digital broadcasters (DAB, DVB) with COFDM modulation," *IEE Proceedings of Radar, Sonar and Navigation*, vol. 152, no. 3, pp. 143–152, June 2005.

[4] D. K. P. Tan, H. Sun, Y. Lu, M. Lesturgie, and H. L. Chan, "Passive radar using global system for mobile communication signal: theory, implementation and measurements," *IEE Proceedings of Radar, Sonar, and Navigation*, vol. 152, no. 3, pp. 116–123, June 2005.

[5] P. E. Howland, D. Maksimiuk, and G. Reitsma, "Fm radio based bistatic radar," *IEE Proceedings of Radar, Sonar and Navigation*, vol. 152, no. 3, pp. 107–115, June 2005.

[6] K. S. Kulpa, "Multi-static entirely passive detection of moving targets and its limitations," *IEE Proceedings of Radar, Sonar, and Navigation*, vol. 152, no. 3, pp. 169–173, June 2005.

[7] C. Coleman and H. Yardley, "Passive bistatic radar based on target illumniations by digital audio broadcasting," *IET Radar Sonar Navig.*, vol. 2, no. 5, pp. 366–375, 2008.

[8] K. Chetty, K. Woodbridge, H. Guo, and G. E. Smith, "Passive bistatic WiMAX radar for marine surveillance," in *Proc. of 2010 IEEE Radar Conference, Washington, DC, USA*, May 2010.
[9] P. Falcone, F. Colone, C. Bongioanni, and P. Lombardo, "Experimental results for OFDM WiFi-based passive bistatic radar," in *Proc. of 2010 IEEE Radar Conference, Washington, DC, USA*, May 2010.
[10] Y. Wu and D. C. Munson, "Multistatic synthetic aperture imaging of aircraft using reflecting television signals," in *Proc. of SPIE, Algorithms for Synthetic Aperture Radar Imagery VIII*, April 2001.
[11] L. Wang, I. Y. Son, and B. Yazıcı, "Passive imaging using distributed apertures in multiple scattering environments," *Inverse Problems*, vol. 26 (065002), 2010.
[12] D. Colton and R. Kress, *Inverse Acoustic and Electromagnetic Scattering Theory*, vol. 93 of *Applied Mathematical Sciences*, Springer, 2 edition, 1998.
[13] D. N. Ghosh Roy and L. S. Couchman, *Inverse Problems and Inverse Scattering of Plane Waves*, Academic Press, London, UK, 2002.
[14] H. H. Barrett and K. J. Myers, *Foundations of Image Science*, Wiley-Interscience, 2003.
[15] M. Cheney and B. Borden, "Imaging moving targets from scattered waves," *Inverse Problems*, vol. 24, pp. 035005(1–22), 2008.
[16] M. Cheney, "A mathematical tutorial on synthetic aperture radar," *SIAM Review*, vol. 43, no. 2, pp. 301–312, 2001.
[17] K. J. Langenberg, M. Brandfass, K. Mayer, T. Kreutter, A. Brüll, P. Felinger, and D. Huo, "Principles of microwave imaging and inverse scattering," *EARSeL Adv. Remote Sens.*, vol. 2, pp. 163–186, 1993.
[18] M. Lax, "Multiple scattering of waves," *Rev. Mod. Phys*, vol. 23, pp. 287–310, 1951.
[19] W. C. Chew, *Waves and Fields in Inhomogeneous Media*, New York: IEEE Press, 1990.
[20] G. Liang and H. L. Bertoni, "A new approach to 3-d ray tracing for propagation prediction in cities," *IEEE Transactions on Antennas Propagat.*, vol. 46, no. 6, pp. 853–863, June 1998.
[21] L. Wang and B. Yazıcı, "Passive imaging of moving targets using sparse distributed apertures," *submitted to SIAM Journal on Imaging Science*.
[22] S. Kay, *Fundamentals of Statistical Signal Processing, Vol. I - Estimation Theory*, Prentice Hall, 1993.
[23] S. Kay, *Fundamentals of Statistical Signal Processing, Vol II - Detection Theory*, Prentice Hall, 1998.
[24] IEEE Std. 802.16e2 005 and IEEE Std. 802.16d2 005, "Part 16: Air interface for fixed and mobile broadband wireless access systems," .

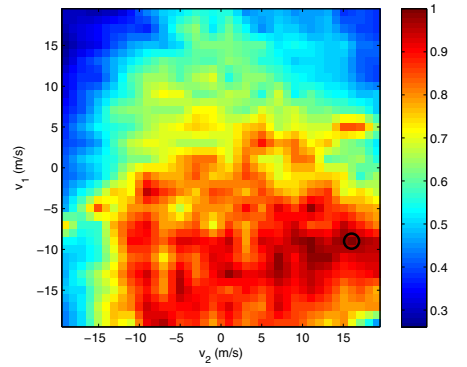

(a)

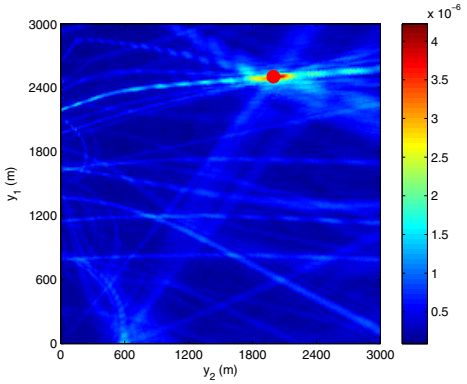

(b)

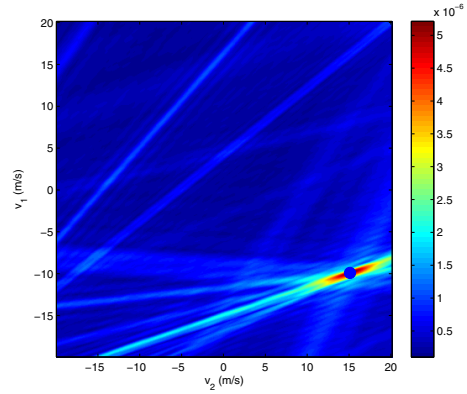

(c)

Fig. 3. The reconstructed images in multiple-scattering environment for a moving point target with 5 receivers and a single transmitter transmitting a high-Doppler and good-range resolution waveform: (a) The peak-value image with the maximum value indicated by a circle. The estimated velocity $\tilde{\boldsymbol{v}} = (-10, 15)\mathrm{m/s}$. (b) The position-image when $\boldsymbol{v} = \tilde{\boldsymbol{v}}$. The estimated position $\tilde{\boldsymbol{y}} = (2500, 2000)\mathrm{m}$. (c) The velocity-image when $\boldsymbol{y} = \tilde{\boldsymbol{y}}$. The circle in (a) indicates the estimated velocity. Solid dots in (b) and (c) indicate the true position and velocity.